Investigation of Boron Nitride Nanomesh Interacting with Water

Ding, Y ; Iannuzzi, M ; Hutter, J

Abstract: Recent scanning tunneling microscopy (STM) experiments have shown that, by dosing liquid water to the bare hexagonal boron nitride (h-BN) nanomesh on Rh(111), water dusters can be observed in the nanomesh pores. With the present work, we intend to better understand the nature of the interaction of water with the nanomesh and give indications on the type of structures that have been observed. To this purpose, the corrugated h-BN monolayer on a 12 x 12 Rh(111) slab is calculated, and its structural and electronic properties are studied in some detail. Then the interaction of small water dusters adsorbed on h-BN, with and without the metal, is investigated. The simulation gives insight into the nature of the binding of h-BN to the metal, the role of the corrugation in trapping molecules, and the structure and distribution of the hydrogen bonds formed by the water molecules. Through simulated STM topography, the optimized structures are compared to the experimental results and the most probable configurations of water aggregates within the pore are identified. The results of our calculations suggest that the water aggregates producing the predominant STM images with three protrusions forming an almost equilateral triangle, with side length of about 0.46 nm, are most likely water hexamers.

Investigation of Boron Nitride Nanomesh Interacting with Water

Yun Ding, Marcella Iannuzzi, and Jürg Hutter[*]

Institute of Physical Chemistry, University of Zurich

Winterthurerstrasse 190 CH-8057 Zurich, Switzerland

Abstract

Recent STM experiments have shown that, by dosing liquid water to the bare *h*-BN nanomesh on Rh(111), water clusters can be observed in the nanomesh pores. With the present work, we intend to better understand the nature of the interaction of water with the nanomesh, and give indications on the type of structures that have been observed. To this purpose, the corrugated *h*-BN monolayer on a 12×12 Rh(111) slab is calculated, and its structural and electronic properties are studied in some details. Then the interaction of small water clusters adsorbed on *h*-BN, with and without the metal, is investigated. The simulation gives insight into the nature of the binding of *h*-BN to the metal, the role of the corrugation in trapping molecules, and the structure and distribution of the hydrogen bonds formed by the water molecules. Through the simulated STM topography, the optimized structures are compared to the experimental results and the most probable configurations of water aggregates within the pore are identified. The results of our calculations suggest that the water aggregates producing the predominant STM images with three protrusions forming an almost equilateral triangle, with side length of about 0.43 nm, are most likely water hexamers.

---
[*]Electronic address: `hutter@pci.uzh.ch`

1

I. INTRODUCTION

The boron nitride nanomesh is a corrugated structure with a periodicity of 3.22 nm, which is formed at high temperature by self-assembly through decomposition of borazine on a Rh(111) surface[1, 2]. The single layer of hexagonal BN shows a regular distribution of 2 nm diameter "pores", separated by regions where the BN layer is less tightly bound to Rh(111), called "wires". Such a corrugation is induced by the lattice mismatch between BN and Rh; the nanomesh unit cell is given by 13×13 BN pairs over 12×12 Rh atoms[2, 3]. The resulting structure turns out to be very stable in gas phase[4], water[2], and various other liquids[5]. In experiment, it has been observed that C_{60}[1] and Naphthalocyanine[2] could be deposited and stabilized in the pore, thus making the nanomesh an interesting candidate as template for self-assembly of ordered and distant molecular lattices. In recent STM experiments, performed after dosing 0.001L water to the empty boron nitride nanomesh at 34K, single and triple protrusions, appearing as bright spots, could be observed as predominant species in some of the pores. These images seem to be associated to trapped water molecules, most probably organized in small 2D clusters. Several hints indicate that the number of water molecules forming these aggregates exceeds the number of visible protrusions. Single protrusions show a diffusion behavior that they may split into double protrusions and back into single protrusions, which indicates that more than one water molecule is present in the pore. Moreover, the analysis of the triple protrusions images revealed that the average distance between these spots is around 4.3 Å, which is close to the distance of second neighbour water molecules in ice clusters. However, the resolution of the collected images does not allow for clear identification of the structures and of the dynamics (aggregation processes, diffusivity) of these water clusters. The experimental evidence tells us that water clusters can be adsorbed in the pore, and they preferentially organize themselves in the structure producing the three protrusions. On the other hand, the fact that on the wire it is much less probable to resolve clear spots showing the presence of adsorbed water molecules, seems to indicate that here the water aggregates are not stable or can easily move and, therefore, cannot be detected by the scanning microscope.

In the present work, we study by means of density functional theory (DFT)[6] the structural and electronic properties of hexagonal boron nitride(*h*-BN) epitaxially grown on Rh(111). A symmetric slab model constituted of a slab of seven 12×12 Rh(111) layers and terminated on both side with one 13×13 *h*-BN monolayer has been considered to investigate the bare nanomesh. We address more specifically the binding interactions between metal and *h*-BN, which are responsible

2

for the variation of the electronic properties between pore and wire. The characterization of the modulation of the work function across the nanomesh, as reported also in experimental works[7], is particularly interesting because it is directly associated to the corrugation and is expected to have an influence on the behavior of adsorbed molecules.

Different water clusters are studied on free standing *h*-BN and on the nanomesh, in order to identify the unresolved structures observed in the experiment. The nature of the binding interactions and the stability of the water aggregates trapped in the pore are addressed. The water hexamer is studied with particular care, since it turns out to provide the best match to the STM picture and it is also the most stable aggregate of water molecules, being the building block for the formation of ice clusters. Possible distortions of the hexamer structure as well as its dynamics on the BN monolayer are also taken into account.

In the following, first some details on the employed computational methods are given. Then the results on the bare nanomesh are reported. The last section is dedicated to the characterization of small water clusters first on free standing BN and finally on the nanomesh.

II. METHOD

ell calculations are performed by DFT, using the Gaussian and plane waves (GPW) formalism[8], as implemented in the CP2K program package[9]. Exchange and correlation are calculated by the revised PBE[10, 11] functional, and corrections for the dispersion interactions are added through the Grimme[12] formalism. Goedecker-Teter-Hutter pseudopotentials[13–15] are used to approximate the interaction of the valence electrons with the atomic cores. In particular, 17 valence electrons are considered for Rh atoms. Double zeta short range basis sets[16] are employed for Rh, B,and N, while triple zeta basis sets are selected to describe O and H. The energy cutoff for the plane waves expansion of the density is set at 500 Ry. The Brillouin zone is sampled only at the Γ point, without loss in accuracy since large simulation cells, containing several hundreds of atoms, are used. For the wavefunction optimization of metallic systems, the Fermi-Dirac smearing of the occupation numbers is applied using 300 K as electronic temperature. Broyden density mixing is used to guarantee smooth convergence within a reasonable number of iterations. Periodic boundary conditions are always applied. The Rh(111) surface is described through a slab model, by adding a sufficient amount of vacuum space (about 20 Å) above the topmost atomic layer, in order to avoid interactions with the periodic images. This simulation

setup has been validated on bulk Rh and the Rh(111) surface, obtaining very good agreement with experiment for several parameters, like the lattice parameter (a=3.780 Å), the bulk modulus (258 GPa), the surface energy (0.19 eV/Å), and the surface work function (5.11 eV). [22]

The optimized structures are characterized in terms of several structural parameters (corrugation, buckling, bond lengths), the adsorption and the interaction energies, the formation of covalent and hydrogen bonding. The modulation of the electrostatic potential above the surface (i.e. the work function) is of particular interest because it is directly related to the corrugation of the nanomesh and it is expected to affect the adsorption of molecules. By the calculation of charge density differences ($\Delta n(\mathbf{r})$) between the full systems and the separated parts (slab and h-BN) the formation of covalent bonding is monitored. Also the density of states projected on selected subsets of atoms (PDOS), and the description of the electronic structure through maximally localized Wannier orbitals (MLWO)[17] are employed as useful analysis tools to investigate the electronic structure rearrangements induced by binding interactions and polarization. The Tersoff-Hamann approximation[18, 19] for STM simulations is used to reproduce the isocurrent topography above the nanomesh. Given a bias potential V_b (typically a fraction of eV), we determine the isocurrent surface as the set of grid points where

$$n_b(z)e^{-2kR_0\sqrt{\Phi(z)}} = \text{const.} \tag{1}$$

In this expression, z is the height above the slab, n_b is the charge density as projected on the states with energies within V_b from the Fermi energy, Φ is the work function, R_0 is an estimate of the tip curvature radius, and $k = \sqrt{2m_e}/\hbar$. By mapping the electrostatic potential on the obtained isocurrent surface, also the experimental dI/dz map can be reproduced and regions with higher or lower work function can be distinguished.

III.   RESULTS AND DISCUSSIONS

A.   Bare nanomesh

It has already been shown in previous works[2, 3, 20] that the lattice mismatch between h-BN (a_0=2.5Å) and Rh(111) (a_0=2.688Å) does not allow a one to one epitaxial growth of h-BN. Coincidence superstructures are formed, instead, with large lattice constants, where the unit cell is a 13×13 h-BN on 12×12 Rh(111). Indeed, the energy payed to stretch the BN bond and match the Rh(111) lattice could not be compensated by the binding to the metal. For free standing, flat

h-BN, we estimate this stretching energy to be more than 0.4 eV per BN pair. On the contrary, the 13×13 *h*-BN on 12×12 Rh(111) superstructure corresponds to an overall contraction of the BN bonds, from 1.45 Å to 1.43 Å (1.4%), with an energy cost of only 0.02 eV per pair.

In order to investigate the properties of the nanomesh, we considered model systems of different size. Preliminary calculations have been carried out with small Rh slabs, constituted of seven 6×6 Rh(111) layers, terminated by stretched and flat 6×6 *h*-BN monolayers on both sides. The lattice parameter for the Rh slabs is set to the experimentally determined value of 3.8 Å. Optimal binding conditions are obtained when N occupies atop sites and B fcc hollow sites. In this case, the *h*-BN monolayer remains flat, at about 2.18 Å over the Rh surface. The interaction with the metal induces the buckling of the BN pairs, with B atoms 0.14 Å closer to the slab surface. The interpretation of the electronic structure through the MLWO representation confirms the presence of binding interaction. For free standing *h*-BN, three MLWO per BN pair are centered along the BN bonds, while a fourth orbital is associated to the lone pair, whose center is very close to the N. On the metal instead, when N occupies the atop site, the lone pair center is clearly displaced into the interlayer region, thus revealing the polarization of the electronic charge due to the interaction with the metal. As a consequence, the *h*-BN monolayer is positively charged and the work function is 3.7 eV, i.e. 1.4 eV smaller than the work function of clean Rh(111). The binding energy calculated with respect to the stretched, free standing *h*-BN is -0.6 eV per pair, whereas the adsorption energy, i.e. the energy gain with respect to free standing *h*-BN at equilibrium, is only -0.14 eV per pair. No binding interaction is observed, instead, when N occupies hollow sites. In the optimized configuration, obtained by laterally constraining the overlayers, *h*-BN remains at more than 2.6 Å from the slab surface. Also the electronic structure of the *h*-BN monolayer is not significantly modified by the presence of the metal, as demonstrated by the fact that all the MLWO associated to BN are centered within the BN plane.

The nanomesh is obtained by employing metallic slabs with seven or four 12×12 Rh(111) layers. The largest system with seven Rh layers is a symmetric slab terminated on both sides by a 13×13 *h*-BN. The structure optimization is carried out relaxing all the degrees of freedom. This sample contains 1008 Rh atoms and 338 BN pairs, corresponding to 19840 valence electrons and 34996 basis functions. The smaller model with only four layers is surmounted by one monolayer on one side only, while the Rh atoms of the bottom layer, on the opposite side, are kept fixed at the bulk positions. This model is used for most of the calculations including also water molecules (the last two Rh layers are fixed in the water system), because of the reduced computational costs; it

5

consists of 576 Rh atoms and 169 BN pairs, corresponding to 11144 valence electrons and 19370 basis functions. It has been verified that the nanomesh properties remain mostly unchanged using the smaller system.

The structure optimization is started from a slightly contracted and flat 13×13 h-BN, in order to match the 12×12 Rh(111) box dimensions. The monolayer is initially located at about 2.5 Å from the Rh surface. The initial Moiré structure is characterized by regions where the N atoms occupy atop sites, i.e. directly on top of Rh atoms, and other regions where they occupy hollow sites, i.e. hcp site on top of an atom of the second Rh layer, or fcc site on top of an atom of the third layer.

Through the optimization of the 13×13 h-BN on 12×12 Rh(111), the expected corrugated structure is obtained. Two approximatively flat regions are clearly distinguished; The pore, where the layer is closer to the metal and the N atoms tend to occupy atop sites, and the wire, about 1 Å more distant from the slab. In the supplementary material, Fig. A(a) reproduces a top view of the replicated corrugated h-BN, where the atoms are colored according to their height above the slab. The pore lays at about 2.2 Å from Rh(111) and corresponds to about 30% of the monolayer. Here bonding between N and Rh is formed, as also indicated by the displacement towards the metal of the MLWO centers corresponding to the N lone pairs (see FIG. 1b). The BN bonds tend to be longer, with average length of 1.46 Å corresponding to a NN distance of 2.53 Å. This elongation favors the effective binding to the metal. For the same reason, the Rh atoms beneath the pore get closer (2.67 Å). The wire lays at about 3.1 Å from Rh and involves more than 50% of the monolayer. The interaction between wire and Rh is weak and dominated by the dispersion contributions, and the boron-nitride electronic charge is not significantly perturbed by the presence of the metal. The average BN bond length here is 1.43 Å or even shorter, to compensate the elongation observed in the pore. The remaining part of the monolayer, 10–15%, forms the intermediate rim that connects pore and wire. The steep change in height, about 1 Å involves only two atomic rows. Fig. A(b) in the supplementary material is a top view of the N lattice that are colored according to the average length of the three BN bonds, thus providing a colored map of the bond length distribution. The map of the height distribution and the map of bond length distribution display quite similar patterns, thus confirming the direct relationship between N binding to the metal and BN bond stretching.

As already mentioned, the strong binding between metal and BN occurs in the pore region only, where the electronic charge of the nitrogen lone pair is polarized towards the metal. A clear picture

of the electronic charge redistribution associated with the binding at the interface is given in FIG. 1a, where the charge density difference $\Delta n(\mathbf{r})$ is displayed. Modification of the charge density due to the interaction are visible only directly below the pore. In the interstitial region we have accumulation of charge coming from the N lone pair and the interfacial Rh layer, thus indicating hybridization of the p states of N with the metallic d band. All over the rest of the systems the electronic charge distribution remains unperturbed. Also the analysis through the MLWO confirms that strong polarization effects involve only the atoms of the pore. In particular, FIG. 1b shows the projected distance d_z between the center of the lone-pair orbital and the corresponding N atom, as computed for the corrugated h-BN on the metal and for the same corrugated structure free-standing in vacuum. While for the free-standing layer, d_z is uniform all over the monolayer ($\approx$ 0.2 Å), a clear increase is recorded for the full system, when N atoms that are closer to the slab, i.e. belonging to the pore. No significant variations have been observed, instead, in the position of the centers of the orbitals along the BN bonds. Hence, the binding is provided by the interaction between N and Rh in the pore through the hybridization of the N lone pair orbitals, with charge polarization towards the metal.

The adsorption energy is computed as $E_{hBN/Rh(111)} - E_{hBN} - E_{Rh(111)}$, where E_{hBN} is the equilibrium energy of free standing h-BN, and $E_{Rh(111)}$ is the energy of the relaxed metallic slab. For the large sample with seven layers, we get -0.33 eV per BN pair [23]. The interaction energy, i.e. $E_{hBN/Rh(111)} - E'_{hBN} - E'_{Rh(111)}$, where E'_{hBN} is the energy of the free standing corrugated h-BN and $E'_{Rh(111)}$ is the energy of the corrugated Rh(111) slab, is -0.39 eV per pair. This latter quantity estimates the pure binding interaction of h-BN with the metal, since the energy costs associated with the contraction, 0.02 eV per BN pair, and the corrugation, 0.04 eV per BN pair, are not subtracted.

In FIG. 2 we report the STM topography, calculated as iso-current surface (see expression 1), obtained with a bias potential of -0.1 eV and the projected density at the center of the mesh equal to 10^{-6}. In the STM image the pore appears as hexagonal depression, 5.2 Å above the slab, i.e. 3 Å above the N atoms. The STM corrugation between pore and wire is about 0.8 Å. From the map of the electrostatic potential computed on this same iso-current surface, the work function variation between pore and wire is 0.5 eV (Fig. B in supplementary material). This can be directly compared to the dI/dz maps reported in experimental work[21]. The modulation of the electrostatic potential, i.e. of the work function, is a direct consequence of the charge density polarization in the pore. Calculating the potential on a plane cutting through the nanomesh, and perpendicularly

to the slab, the estimate of variation between higher values above the wire and lower values above the pore is of about 0.6 eV (FIG. 3). This feature of the nanomesh is of particular interest, because such gradient in the electrostatic potential may act as a trapping well for adsorbed molecules. It is also worth to notice that a modulation of about the same amount is present above the corrugated, free standing h-BN, but it is inverted, being the potential higher over the pore.

Finally, the density of states projected on the N_{p_x} states presents clear features related to the presence of non equivalent N atoms, i.e. atoms that bind directly to the metal and others only weakly interacting with the slab. Projecting the DOS only on the N atoms in the pore or only on the N atoms of the wire region, the specific features associated to each type can be identified. In particular, two bands about 6 eV below the Fermi energy and separated by about ~1 eV are distinguished (see Fig. C in supplementary material), in agreement with experiment and previous calculations [1, 3, 20].

B.   Nanomesh with water deposition

In order to identify the water aggregates that are observed in the experiment as three protrusions of the STM topography, several water clusters have been investigated.

First, the structures of water aggregates, from the monomer to different possible isomers of the hexamer, have been optimized on a flat, free standing 8×8 BN monolayer, comparing different possible adsorption sites. In all the studied cases, we observe that the binding to BN is rather weak (on average less than -0.16 eV per molecule) and the h-bond interactions (OH$\cdots$O) between the molecules themselves are dominant. The interaction with the substrate occurs mainly through h-bonds of the type OH$\cdots$N. In Tab. I, the adsorption energy per H_2O molecule with respect to the same cluster optimized in vacuum, the number of h-bonds of type OH$\cdots$O and OH$\cdots$N, as well as their average length are reported for the most stable configurations of each cluster type.

This first set of calculations confirms that water molecules deposited on BN tend to pack in order to maximize the number of internal h-bonds. The resulting nearest OO distance is typically about 2.7 Å, i.e. much shorter than the distance measured between the STM protrusions. However, in the case of the regular hexamer, selecting every second molecule of the ring, the O atoms form an almost equilateral triangle, where the OO distance is ≈4.6 Å. This picture approximatively matches with the triangle formed by the three STM protrusions in the pore. The hexamer seems also to be the optimal building block for aggregation of water molecules on BN. Indeed, by adding

TABLE I: Water clusters adsorbed on free standing BN: adsorption energy, number and average length of hydrogen bonds

	E_{ad}	OH$\cdots$O		OH$\cdots$N	
	[eV/H$_2$O]	n	$\bar{d}$ [Å]	n	$\bar{d}$ [Å]
monomer[a]	-0.158	-	-	2	3.36
dimer[a]	-0.137	1	2.91	2	3.32
trimer	-0.108	3	2.86	2	3.39
tetramer	-0.093	4	2.75	2	3.51
pentamer	-0.096	5	2.73	3	3.43
hexamer	-0.086	6	2.71	3	3.28

[a]Other possible adsorption configurations for the water monomer and the water dimer involve the formation of only one OH$\cdots$N h-bond, with a length of 3.30 Å for both cases. The water molecules are about 0.1 Å closer to BN, and E_{ad} differ by only 0.001 eV/H$_2$O.

one molecule close to the hexamer, it binds to the ring through a h-bond, but remaining only externally attached. The most stable structure of the hexamer on BN is the regular hexamer, placed parallel to the layer at a distance of about 3.3 Å. It is characterized by three molecules (position 1, 3, and 5 in the ring) forming one strong OH$\cdots$O h-bond (2.72 Å) with the next molecule in the ring and one weak OH$\cdots$N h-bond with the closest N atom (3.28 Å). The other three molecules form only one OH$\cdots$O h-bond, while their second hydrogen is dangling outward (with respect to BN). The O atoms with one dangling hydrogen are slightly higher over the BN plane (O buckling of 0.14 Å). It is worth noting that the regular hexamer also corresponds to the lowest dipole moment, since the molecular dipoles optimally compensate each other within the ring geometry. From the MLWO analysis, a total cluster dipole of 0.386 D has been calculated. By displacing the cluster parallel to the BN plane, it is possible to find alternative stable configurations, where the OH$\cdots$N are re-oriented by switching to a different neighboring N. Hence, several possible configurations of the hexamer can be optimized, which differ for the relative position with respect to the BN layer and for the length and orientation of OH$\cdots$N. These differences may induce small deformations of the hexamer, which can be quantified in terms of the chirality defined as

$$\xi = \frac{|(a-b)(b-c)(c-a)|}{(a+b+c)^3} \tag{2}$$

9

where a,b,c are the distances between two second neighbor oxygen atoms (i.e. those forming the triangle). The corresponding changes in adsorption energy are also small, i.e. less than 0.01 eV per H_2O. By running molecular dynamics (MD) simulations at relatively low temperature, 150 K, the easy switching of the h-bond from one N to the next turns out to favor the free diffusion of the hexamer parallel to h-BN. We observe that the hexamer moves by undergoing structural distortions when one switching process occurs, but always keeping its two dimensional hexagonal form. Along the MD trajectory, the six OH$\cdots$O h-bonds are stable and prove to be quite rigid, allowing thermal fluctuations of OO distances of about 0.3 Å. The molecules binding to the substrate keep always the same orientation, i.e. with one H pointing to the layer and one to the next molecule of the ring. The dangling hydrogen of the other three molecules, instead, is free to rotate, taking outward, parallel, and inward positions.

Next we study some water aggregates on the nanomesh formed by the 13×13 BN on a 4-layer 12×12 Rh(111) slab, collocating a few water molecules in the pore or on the wire. As already described above, the BN electronic charge distribution in the pore is modified due to the binding interactions between N and Rh, making the N atoms more positively charged. On the other hand, the modulation of the electrostatic potential due to the corrugation may act as a trapping potential well. We want to understand how the corrugation may affect the properties of the adsorbed clusters, and compare the simulated STM images to the experimental data to give hints on the observed structures. In Tab. II, we report the adsorption energy, the number and the average length of the h-bonds calculated for the optimized clusters.

The water monomer optimized in the pore does not form any OH$\cdots$N bonds. On the contrary, the negative charge of the O lone pair is attracted by electron-deficient B atoms and the OB distance is 3.02 Å. As a consequence, the two OH are one pointing outward and the other parallel to the surface. On the wire, the adsorption pattern of the water monomer is more similar to the binding on a flat BN surface. One of the proton is pointing to the N atom, forming a OH$\cdots$N bond 3.38 Å long. The other OH is parallel to the surface. Despite the two structure optimizations have been initiated from the same geometry, two different configurations are obtained. This difference can be explained considering the polarization of the lone pair of the nitrogen in the pore, thus leaving less negative charge on the BN surface, which could stabilize the proton. The water monomer is stable also close to the rim of the nanomesh, where one proton points to the nearby nitrogen, forming a OH$\cdots$N h-bond 3.17 Å long. The other OH, instead, points outwards. The O atom is almost on top of the boron, and the OB distance is 3.14 Å. Because of the attractions between the

TABLE II: Water clusters on nanomesh: adsorption energy, number and average lengths of hydrogen bonds

	E_{ad}	OH$\cdots$O		OH$\cdots$N	
	[eV/H$_2$O]	n	$\bar{d}$ [Å]	n	$\bar{d}$ [Å]
monomer(pore)	-0.146	-	-	-	-
monomer(wire)	-0.118	-	-	1	3.38
monomer(rim)	-0.196	-	-	1	3.17
dimer(pore)	-0.151	1	2.89	2	3.26
dimer(wire)	-0.142	1	2.91	2	3.31
trimer(pore)	-0.075	3	2.84	1	3.14
hexamer(pore)	-0.117	6	2.73	3	3.45
hexamer(wire)	-0.066	6	2.72	3	3.44
hexamer(rim)	-0.106	6	2.72	3	3.31

oxygen and boron, and the formation of the OH$\cdots$N h-bond, this structure has a lower adsorption energy compared to the two other adsorption sites. Starting from an initial position exactly on the rim, where the electrostatic potential has a gradient, we observe that during the optimization the water monomer moves closer to the center of the pore. However, it could keep the h-bond to the same nitrogen during the optimization, and once the oxygen is on top of the boron atom, it stays there. The further sliding towards the pore would require an activation energy to break this h-bond. Being this a weak interaction, we expect that at finite temperature the molecule would easily move down to the center of pore, where the electrostatic potential has its minimum.

Things change for the water dimer in the pore. The h-bond donor oxygen is not forming h-bonds to the surface, i.e. its dangling H points outwards, while the negatively charged lone pair is closer to the surface. The other oxygen, instead, offers its lone pair to form the OH$\cdots$O h-bond, while the positively charged protons point to two different N, forming weak h-bonds with NH length of 2.49 and 2.51 Å. The water dimer adsorbed on the wire shows a very similar configuration as in the pore.

The STM topography calculated for the sample with the monomer in the pore and the one with the dimer in the pore shows that water molecules differently oriented with respect to the surface generate pretty dissimilar images. Namely, the STM simulations are carried out with a negative biasing potential, i.e. we sample the occupied states close to the Fermi energy. Hence,

11

the electronic cloud of the oxygen lone pair sticks out, when it is not hidden by other parts of the molecule. As a result, in the STM image generated for the water monomer (FIG. 4a), where the lone pair is closer to the surface and the OH point outwards, no protrusion is appearing. In the case of the dimer, instead, we clearly distinguish one protrusion, as displayed in FIG. 4b, corresponding to the oxygen of the acceptor molecule, i.e. the one forming the OH$\cdots$N h-bonds. According to this picture, the STM may provide more information than expected on the configuration of water aggregates, discriminating among molecules, depending on the position of the hydrogens. It also indicates that the three protrusions observed in the experiment should not be associated to three water monomers.

To rule out the possibility that three separated monomers, about 4.6 Å distant from each other, may be stabilized in the pore and generate the three protrusions image, three molecules have been placed in such configuration and then the structure has been optimized. The optimization brings the three molecules together, to form a trimer, where three OH$\cdots$O h-bonds are formed, and the average OO distance is 2.84 Å. In the final configuration, only one molecule forms a OH$\cdots$N h-bond to the surface, which is 3.18 Å long. The second H of the other two molecules, instead, is dangling and pointing outwards. Hence, while the dimer forms two OH$\cdots$N bonds, with distances of 3.26 Å, the trimer has only one of such interactions. That's the reason why the binding divided by the number of water molecules for the water trimer is much weaker as compared to the dimer. The STM topography calculated for the trimer shows only one protrusion, corresponding to the only molecule with no dangling H and with exposed lone pair (FIG. 4c).

The hexamer optimized in the pore forms three OH$\cdots$N of length 3.39, 3.47 and 3.49 Å, while the average OH$\cdots$O distance is 2.73 Å. Although the hexamer is not perfectly symmetric after geometry optimization, the difference of the OO distance is relatively small. The atomic OO distances among the pointing-down water molecules are 4.68, 4.71 and 4.76 Å, corresponding to chirality $\xi = 4.97 \times 10^{-8}$. The distances between the other three molecules are 4.68, 4.71 and 4.77 Å. The corresponding STM image, as reported in FIG. 5a, shows three protrusions at distances 4.95, 4.97, and 4.99 Å, i.e. with very little distortion with respect to an equilateral triangle. The chirality ξ_{STM}, as computed with respect to the centers of the three spots, is 4.93×10^{-9}, i.e. considerably smaller than the average chirality measured from the experimental STM images. The influence of the Rh layers on the electronic structure of the water hexamer is relatively small. In Tab. III we report the dipole values calculated for the water hexamer in the pore of the nanomesh, on the wire, and in the pore of free-standing, corrugated BN. We find that without the metal the

dipole is 0.118 Debye, i.e. smaller than the 0.724 Debye computed in the pore of *h*-BN/Rh(111). However, in all cases, the dipole moments are quite small in all directions.

TABLE III: Values of the dipole moment along the three cartesian directions, computed for the water hexamer above the free standing corrugated BN and above the nanomesh. The dipole moments are obtained from the positions of the atomic nuclei and of the centers of the MLWO

	Dipole Moment (Debye)			
	μ_x	μ_y	μ_z	$|\mu|$
hex_corrugated BN	0.038	-0.111	-0.011	0.118
hex_pore	-0.0105	-0.133	-0.712	0.724
hex_wire	0.027	-0.200	-0.133	0.242

The hexamer can be optimized in a stable configuration also on the wire. Here, it forms three OH$\cdots$N h-bonds of length 3.29, 3.42, and 3.61 Å, which are in average shorter than in the pore as the nitrogen atoms on the wire are more negatively charged. The average OO distance is 2.72 Å, i.e. very close to the value calculated for the water hexamer in the pore. The OO distances between the water molecules pointing down are 4.66, 4,70 and 4.79 Å, corresponding to chirality $\xi = 1.41 \times 10^{-7}$. The hexamer optimized on the wire is only 0.05 eV per water molecule less binding than in the pore, showing a preference of this cluster to be adsorbed in the pore. However, we already observed that such small variations in binding energy can be obtained by moving or distorting the hexamer just a little, so that the h-bond to the substrate switch from one to another N atom and are partially re-oriented.

There must be water molecules invisible to experimental STM, and the results collected up to now suggest that the most frequently observed cluster could be the cyclic water hexamer, where every second molecule is oriented inward, i.e. h-bonded to the surface, and therefore can be seen as protrusion in the topography. However, most of the experimental three protrusions images are characterized by a quite larger chirality, with the magnitudes of 10^{-6} to 10^{-3}. One possible origin of this distortion is the presence in the pore of other molecules interacting with the hexamer, but not visible for the STM, or even the interaction of the tip of the microscope. We are not going to explore these possibilities in this work, but we consider the effect of the rim and of small displacements of the hexamer with respect to the substrate.

By placing the hexamer over the rim of the nanomesh, the optimized structure has still three

molecules binding to the surface by OH$\cdots$N interactions, and the triangle formed by the three oxygens is indeed more distorted, with OO distances of 4.56, 4.84 and 4.70 Å, and $\xi = 2.06 \times 10^{-6}$. In contrast to the hexamer in the pore, on the rim the height of the molecules variates by about 1 Å, following the corrugation of the BN layer to better orient the OH and optimize the OH$\cdots$N binding. The resulting three OH$\cdots$N h-bonds have lengths of 3.24, 3.27 and 3.41 Å, i.e. tendentially shorter than in the pore, thus explaining the similar adsorption energy, -0.106 eV per water molecule, in spite of the distorsion. The distortion is also visible in STM image (shown in FIG. 5b), where the three protrusions are at distances 4.82, 5.02 and 5.24 Å, and ξ_{STM} is 5.37×10^{-6}. The fact that the water hexamer might also be adsorbed at the rim of the nanomesh is consistent with experiment, where water aggregates generating three protrusions close to the rim have been observed. The chirality of the calculated geometry, however, is still smaller than the one resulting from the experimental image.

From the MD trajectory of the hexamer on flat BN, we selected two configurations of the cluster that turn out to be stable, in spite of the larger distortion of the ring. The distortion occurs when the cluster is diffusing over the monolayer and, in order to favor the formation of the OH$\cdots$N h-bond, one or two molecules of the ring are displaced to reach for nitrogens that are farther apart. This condition is also associated with a larger angle formed by the OH with respect to the normal of the BN plane. The two selected geometries optimized on the flat BN correspond to a chirality of 9.63×10^{-8} and 2.44×10^{-6}, respectively. We expect that the same geometry should generate even more distorted STM images once located in the pore of the nanomesh, because the position of the protrusions depends also on the orientation of the OH bond pointing to the substrate. Then, we have tried to reproduce the same configurations on nanomesh, choosing a location that could preserve as much as possible the same distances between atoms of the cluster and atoms of the substrate. Without performing any structure optimization, we have computed the STM topography for the frozen configurations and, as expected, asymmetric STM images are obtained. As expected, the distortion given by the protrusions is significantly larger, corresponding to chirality 1.23×10^{-6} and 6.54×10^{-7}. Further investigation of the interaction between water and the nanomesh should consider the dynamics of the clusters on the full substrate, in order to address the formation of the aggregates and their diffusivity at finite temperature. In particular, we are interested in comparing the diffusivity in the pore and on the wire, because we believe that the fact that these structures are always observed in the pore is due to the trapping effect of the electrostatic potential well as determined by the corrugation. It is important to remark, that all these cluster lay quite high above

the substrate, with the O atoms about 3 Å distant from the BN plane. This means that the water molecules above the pore are higher than the wire, and their movement cannot be hindered by the structural corrugation (only 1 Å.) These and other aspects related to the dynamics of water on the nanomesh will be the subject of future work.

IV. CONCLUSION

We presented a DFT study of the hexagonal boron nitride nanomesh, showing that our model for this complex interface system is in very good agreement with the experimental observation. Our simulations reproduce the corrugated BN on Rh(111) without the need of imposing any constraint to the system, giving values of the STM corrugation and of the variation of the work function very close to what is measured in experiment. Charge density differences and MLWO analysis show that binding between the h-BN and Rh(111) is present only within the pore region, elsewhere the interaction is dominated by dispersion forces. In particular, comparing the electronic structure and the modulation of the electrostatic potential of the nanomesh to what obtained for the corrugated free standing BN suggests that the polarization effects induced by the interaction with the metal are crucial in determining the right environment to trap molecules in the pore.

Motivated by recent experimental results showing the formation of stable structures by dosing water to the nanomesh, we extended our investigation to the interaction of the nanomesh with water molecules and small water clusters. From our geometry optimization and the STM image calculations, we conclude that the frequently observed three protrusion images are related to the presence of hexamer clusters trapped in the pore. The distance between the protrusions and the fact that only certain molecules appear in the STM topography, leads us to exclude that these images could be associated to a water trimer. Since the STM topography highlights those molecules exposing the negatively charged O lone pair, we cannot rule out the existence of more water molecules in the pore. However, our results suggest that the smallest aggregate that can give rise to the characteristic three protrusion image is most probably the water hexamer. Besides, the geometry optimization of a seventh water molecule added to the water hexamer on a flat BN surface didn't break the cyclic hydrogen bond structure of the water hexamer. Certain experimental images also indicate the possible presence of more molecules, due to the strong distortion of the triangle formed by the protrusions, and also due to light shadows around the main spots, which are visible in the image. All the evidence, however, seems to indicate that when small amount of water

15

is present, the three spots structure is the most favorable pattern. This work provides important hints about the structure of the water clusters in the pore and on the interpretation of the STM images. As indicated by our MD simulations of the water hexamer over the free-standing flat BN, it's quite possible the molecules can easily diffuse over the flat region of the wire. In this case, their aggregation might be hindered, or anyway the detection by STM of the moving aggregates is not possible. On the other hand, within the pore the diffusivity might be substantially reduced due to the trapping effect of the modulated electrostatic potential. Much is still to be understood about the properties and dynamics of water aggregates on the nanomesh. We plan to continue our research on this topic by extending our study to molecular dynamics simulations that reproduce the important processes associated with these systems.

References

[1] M. Corso, W. Auwarter, M. Muntwiler, A. Tamai, T. Greber, and J. Osterwalder. Boron Nitride Nanomesh. *Science*, 303(5655):217–220, 2004.

[2] S. Berner, M. Corso, R. Widmer, O. Groening, R. Laskowski, P. Blaha, K. Schwarz, A. Goriachko, H. Over, S. Gsell, M. Schreck, H. Sachdev, T. Greber, and J. Osterwalder. Boron nitride nanomesh: Functionality from a corrugated monolayer. *Angewandte Chemie-International Edition*, 46(27):5115–5119, 2007.

[3] Robert Laskowski, Peter Blaha, Thomas Gallauner, and Karlheinz Schwarz. Single-layer model of the hexagonal boron nitride nanomesh on the rh(111) surface. *Phys. Rev. Lett.*, 98(10):106802, 2007.

[4] O. Bunk, M. Corso, D. Martoccia, R. Herger, P. R. Willmott, B. D. Patterson, J. Osterwalder, I. van der Veen, and T. Greber. Surface x-ray diffraction study of boron-nitride nanomesh in air. *Surface Science*, 601(2):L7–L10, 2007.

[5] R. Widmer, S. Berner, O. Groning, T. Brugger, E. Osterwalder, and T. Greber. Electrolytic in situ stm investigation of h-bn-nanomesh. *Electrochemistry Communications*, 9(10):2484–2488, 2007.

[6] W. Kohn and L. J. Sham. Self-consistent equations including exchange and correlation effects. *Physical Review*, 140(4A):A1133–A1138, 1965.

[7] H. Dil, J. Lobo-Checa, R. Laskowski, P. Blaha, S. Berner, J. Osterwalder, and T. Greber. Surface trapping of atoms and molecules with dipole rings. *Science*, 319(5871):1824–1826, 2008.

[8] G. Lippert, J. Hutter, and M. Parrinello. A hybrid gaussian and plane wave density functional scheme. *Molecular Physics*, 92(3):477–487, 1997.

[9] CP2K version 2.0.1(Development Version), the CP2K developers group (2009). CP2K is freely available from http://cp2k.berlios.de/.

[10] J. P. Perdew, K. Burke, and M. Ernzerhof. Generalized gradient approximation made simple. *Physical Review Letters*, 77(18):3865–3868, 1996.

[11] Y. K. Zhang and W. T. Yang. Comment on "generalized gradient approximation made simple". *Physical Review Letters*, 80(4):890–890, 1998.

[12] S. Grimme. Semiempirical gga-type density functional constructed with a long-range dispersion correction. *Journal of Computational Chemistry*, 27(15):1787–1799, 2006.

[13] S. Goedecker, M. Teter, and J. Hutter. Separable dual-space gaussian pseudopotentials. *Physical Review B*, 54(3):1703–1710, 1996.

[14] C. Hartwigsen, S. Goedecker, and J. Hutter. Relativistic separable dual-space gaussian pseudopotentials from h to rn. *Physical Review B*, 58(7):3641–3662, 1998.

[15] M. Krack. Pseudopotentials for h to kr optimized for gradient-corrected exchange-correlation functionals. *Theoretical Chemistry Accounts*, 114(1-3):145–152, 2005.

[16] J. VandeVondele and J. Hutter. Gaussian basis sets for accurate calculations on molecular systems in gas and condensed phases. *Journal of Chemical Physics*, 127:114105, 2007.

[17] Arash A. Mostofi, Jonathan R. Yates, Young-Su Lee, Ivo Souza, David Vanderbilt, and Nicola Marzari. wannier90: A tool for obtaining maximally-localised wannier functions. *Computer Physics Communications*, 178(9):685 – 699, 2008.

[18] J. Tersoff and D. R. Hamann. Theory and application for the scanning tunneling microscope. *Physical*

Review Letters, 50(25):1998–2001, 1983.

[19] J. Tersoff and D. R. Hamann. Theory of the scanning tunneling microscope. *Physical Review B*, 31(2):805–813, 1985.

[20] R. Laskowski and P. Blaha. Unraveling the structure of the h-BN/Rh(111) nanomesh with ab initio calculations. *Journal of Physics-Condensed Matter*, 20(6), 2008.

[21] H. F. Ma, T. Brugger, S. Berner, Y. Ding, M. Iannuzzi, J. Hutter, J. Osterwalder, and T. Greber. Nano-ice on boron nitride nanomesh: Accessing proton disorder. *Chemphyschem*, 11(2):399–403, 2010.

[22] The bulk calculations are performed with a $6\times6\times6$ cubic box containing 864 Rh atoms. The Rh(111) surface has been modeled by a slab of seven 12×12 Rh(111) layers, for a total of 1008 atoms, using the experimental lattice constant, 3.8 Å.

[23] It is interesting to notice that by displacing *h*-BN relative to Rh(111), we could optimize structures with slightly different geometries within the pore, even if the corresponding differences in adsorption energy are smaller than 0.01 eV per BN. In particular, the pore with N-top and B-fcc is lower in energy than the N-top and B-hcp configuration, while the structure with pore centered on three equivalent atop N atoms is 0.01 eV per BN pair lower in energy than the structure with pore centered on one N only. In all cases height distribution over Rh, the extension of the pore, as well as the electronic properties do not present significant differences.
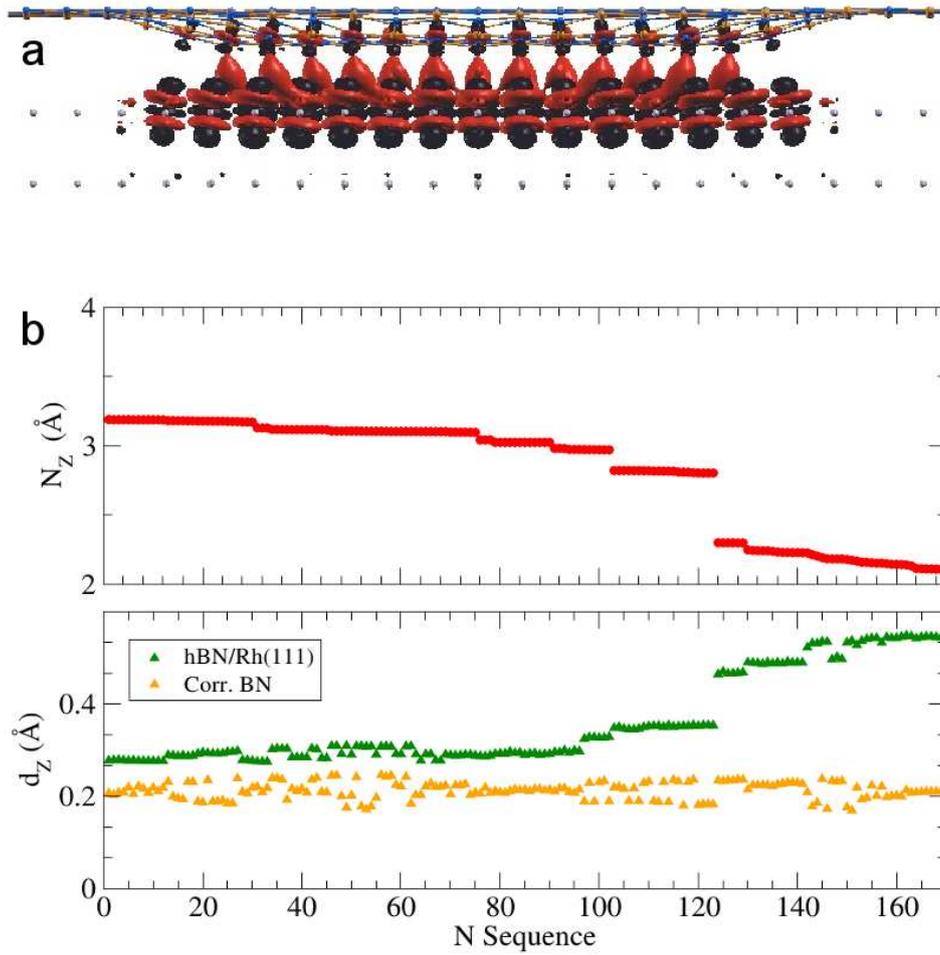
FIG. 1: **a**. The total charge density difference between the nanomesh and sum of the free standing BN and the Rh slab. The red indicates the accumulation of the charge density, while the black stands for the diffusion of the charge density. **b**. Distance of N atoms from the top layer Rh along z axis (upper panel) and the corresponding distance of the MLWO centers of the N lone pair from its nucleus for nanomesh (green) and the corrugated BN (orange) (lower panel).
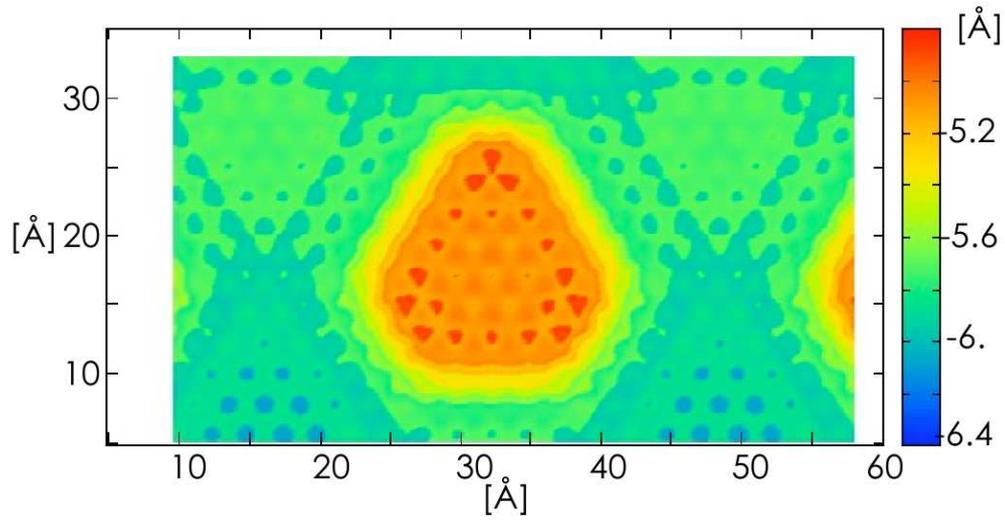
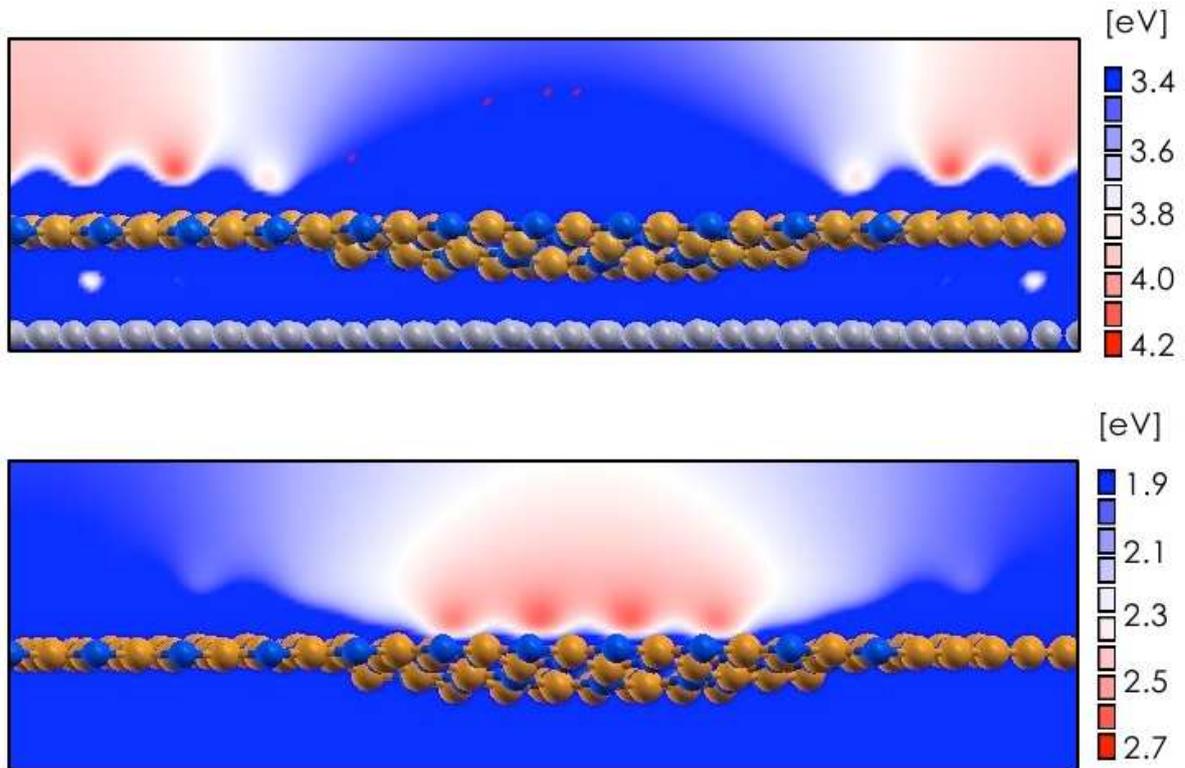FIG. 2: Calculated STM topography for nanomesh at a density of 10^{-6}.

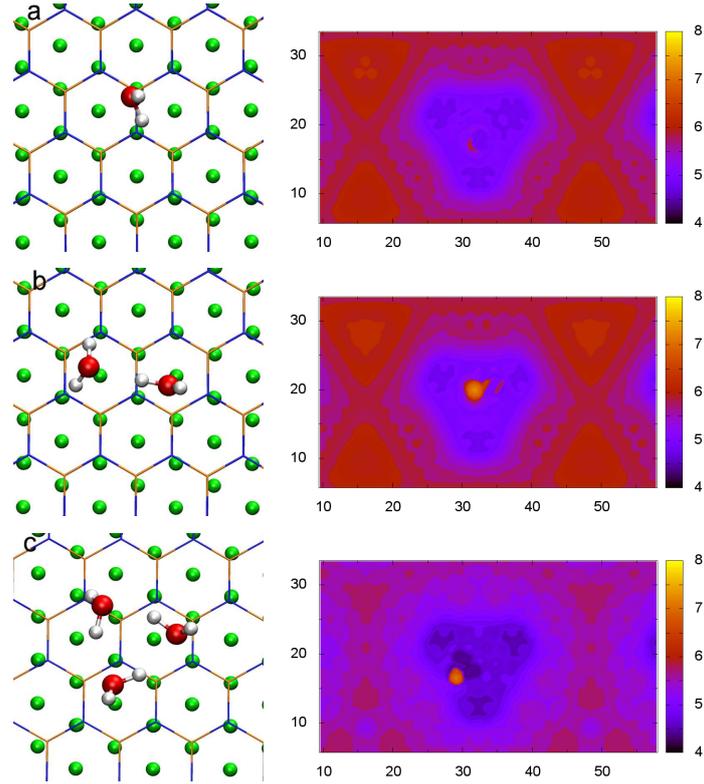FIG. 3: Electrostatic potential images of the nanomesh (upper) and the corrugated BN only (lower).

20

FIG. 4: Configurations (left column) and the corresponding STM topography images (right column, all values are in Å) for water monomer (**a**), water dimer (**b**) and water trimer (**c**) in the pore of the nanomesh. All the images are generated at the bias of -0.1 eV with $n_b=10^{-6}$ and $R_0=4$ Å.
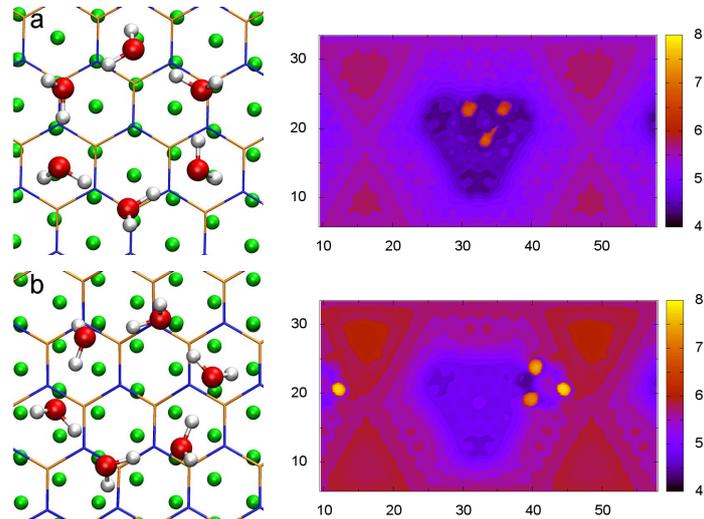

FIG. 5: Configurations (left column) and the corresponding STM topography images (right column, all values are in Å) for water hexamer in the pore of the nanomesh (**a**) and also water hexamer on the rim of the nanomesh (**b**). All the images are generated at the bias of -0.1 eV with $n_b=10^{-6}$ and $R_0=4$ Å.